Tectonic geomorphological investigations of antiforms using differential geometry: Permam anticline, northern Iraq

Annegret Burtscher, Marcel Frehner, and Bernhard Grasemann

ABSTRACT

Modern differential geometric methods are applied to compute and analyze curvature quantities of the Permam anticline, which is part of the Zagros fold and thrust belt in northern Iraq, northeast of the city of Erbil. Because this particular anticline is composed of, among others, weathering-resistant limestones, the surface topography strongly resembles the antiformal fold shape. This makes it an ideal area where numerical curvature analysis, applied to Shuttle Radar Topography Mission digital elevation models (DEMs), allows drawing not only geomorphological, but also tectonic, conclusions. The curvature analysis is based on the computation of the Gaussian and mean curvatures and is used to classify the folded surface into eight geologically relevant shapes (antiform, synform, plane, dome, basin, and three types of saddles). The performed curvature analysis investigates in detail the effects of two adaptable parameters: the cutoff wavelength of the low-pass filter that is applied to the DEM before curvature calculation and the curvature threshold that is applied to the principal curvature values before the calculation of the Gaussian and mean curvatures. The analysis demonstrates that these two parameters strongly influence each other, and that they together determine the information content and interpretability of the results. By choosing appropriate parameter combinations, geomorphological-oriented studies and tectonic-oriented studies are viable using the same DEM. How tectonic-oriented studies can be used to determine fracture patterns or densities in folded layers is discussed. Further suggestions are made to combine curvature analysis of DEMs

Manuscript received December 20, 2010; provisional acceptance March 10, 2011; revised manuscript received May 23, 2011; final acceptance June 14, 2011.
DOI:10.1306/06141110204

AUTHORS

ANNEGRET BURTSCHER ~ *Faculty of Mathematics, University of Vienna, Austria, Nordbergstraße 15, 1090 Vienna, Austria*

Annegret Burtscher is a mathematician pursuing her Ph.D. at the University of Vienna (Austria) and Université Pierre et Marie Curie (Paris VI, France). She received an M.S. degree in mathematics and a B.S. degree in earth sciences from the University of Vienna. Her research interest is differential geometry, in particular, Riemannian geometry and geometric applications to geology.

MARCEL FREHNER ~ *Department for Geodynamics and Sedimentology, University of Vienna, Austria, Althanstraße 14, 1090 Vienna, Austria*

Marcel Frehner is a university assistant at the Geological Institute of ETH Zurich (Switzerland). He received his Ph.D. in earth sciences from ETH Zurich, after which he spent some time as a university assistant at the University of Vienna (Austria). M. Frehner specializes on numerical simulations and quantitative analysis of geologic and geodynamical processes.

BERNHARD GRASEMANN ~ *Department for Geodynamics and Sedimentology, University of Vienna, Austria, Althanstraße 14, 1090 Vienna, Austria*

Bernhard Grasemann received his Ph.D. in geology from the University of Vienna. He studied the geodynamic evolution of the Himalayas and the Hellenides in several international projects. Since 2007, he has been a professor in geodynamics at the University of Vienna. His scientific interests include the evolution of mountain belts and the quantification of structural processes at various scales.

ACKNOWLEDGEMENTS

We thank David D. Pollard, Peter Hennings, and an anonymous referee for thorough reviews. This work was supported by the OMV Exploration and Production GmbH. Annegret Burtscher was supported by research fellowship 506/2010 of the University of Vienna and FWF-project P20525 of the Austrian Science Fund.
The AAPG Editor thanks the following reviewers for their work on this paper: Peter Hennings, David D. Pollard, and an anonymous reviewer.

with similar studies applied to seismically mapped surfaces in three-dimensional seismic data sets where erosion is absent.

INTRODUCTION

Geologic surfaces, such as the top of a sedimentary formation, may be deformed into complex shapes, which can be quantitatively described by differential geometry (e.g., surface curvature, convexity, local maximums and/or minimums, saddle and inflection points). Curvature analysis has been used to describe the geometry of geologic structures (Lisle and Robinson, 1995; Pollard and Fletcher, 2005; Mynatt et al., 2007; Fernandez-Martínez and Lisle, 2009; Lisle et al., 2010), to quantify strain (Samson and Mallet, 1997; Johnson and Johnson, 2000), to predict fracture orientations or densities (Hennings et al., 2000; Stephenson et al., 2007), or to analyze geomorphological features (Bergbauer and Pollard, 2003; Jordan, 2003). Most of these studies use the Gaussian curvature, k_G (i.e., the product of the two principal curvatures), and/or the mean curvature, k_M (i.e., the average of the two principal curvatures), to define the shape and orientation of the geologic surface. By combining the information of the Gaussian and mean curvatures, Mynatt et al. (2007) introduced the so-called geologic curvature, which describes eight fundamental shapes (Figure 1) that are relevant for the description of geologic structures (Roberts, 2001; Lisle, 2004; Pollard and Fletcher, 2005).

The quantitative description of geologic surfaces has motivated several geophysical studies with the aim of predicting rock properties of subsurface units. For example, particular geometric attributes of geologic structures have been used for fracture density prediction within hydrocarbon reservoirs (Lisle, 1994; Fischer and Wilkerson, 2000; Stephenson et al., 2007) or for automatic fault detection (Lisle, 1994; Roberts, 2001; Bergbauer et al., 2003). Based on these ideas, this article presents the analysis of the antiformal and synformal structures of a part of the Zagros fold and thrust belt by means of differential geometry. This mountain chain contains 49% of the global fold-and-thrust belt–related hydrocarbons and has, therefore, attracted numerous recent studies (Lacombe et al., 2007; Ries et al., 2007, and references therein).

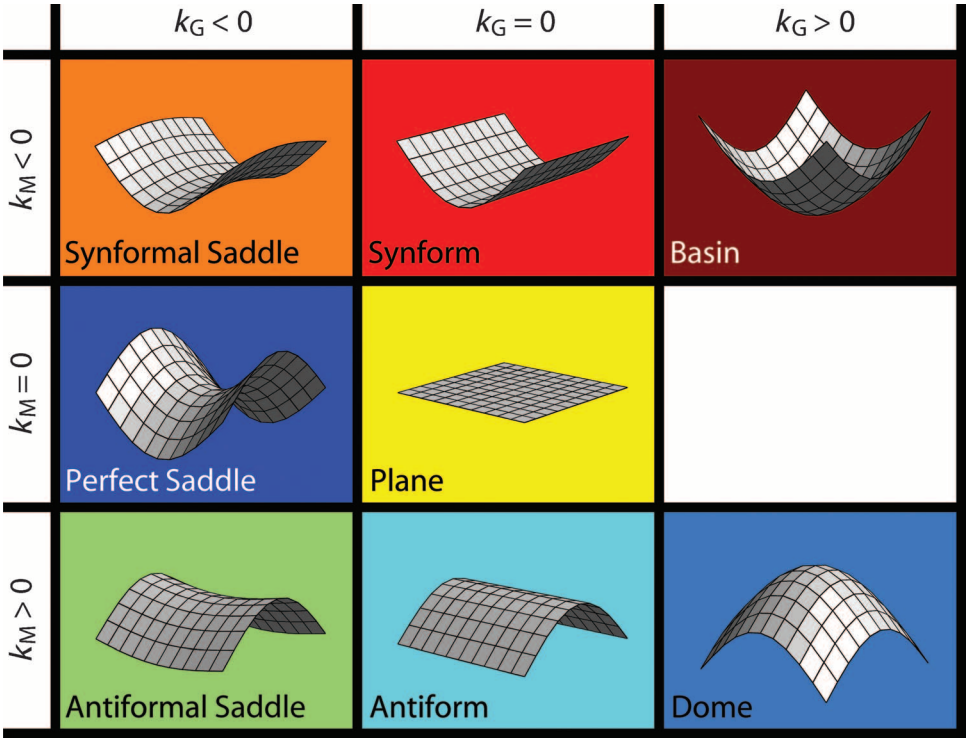

Figure 1. Geologic curvature classification based on the relation of Gaussian (k_G) and mean (k_M) curvature (modified from Mynatt et al., 2007) and color scheme used in this article.

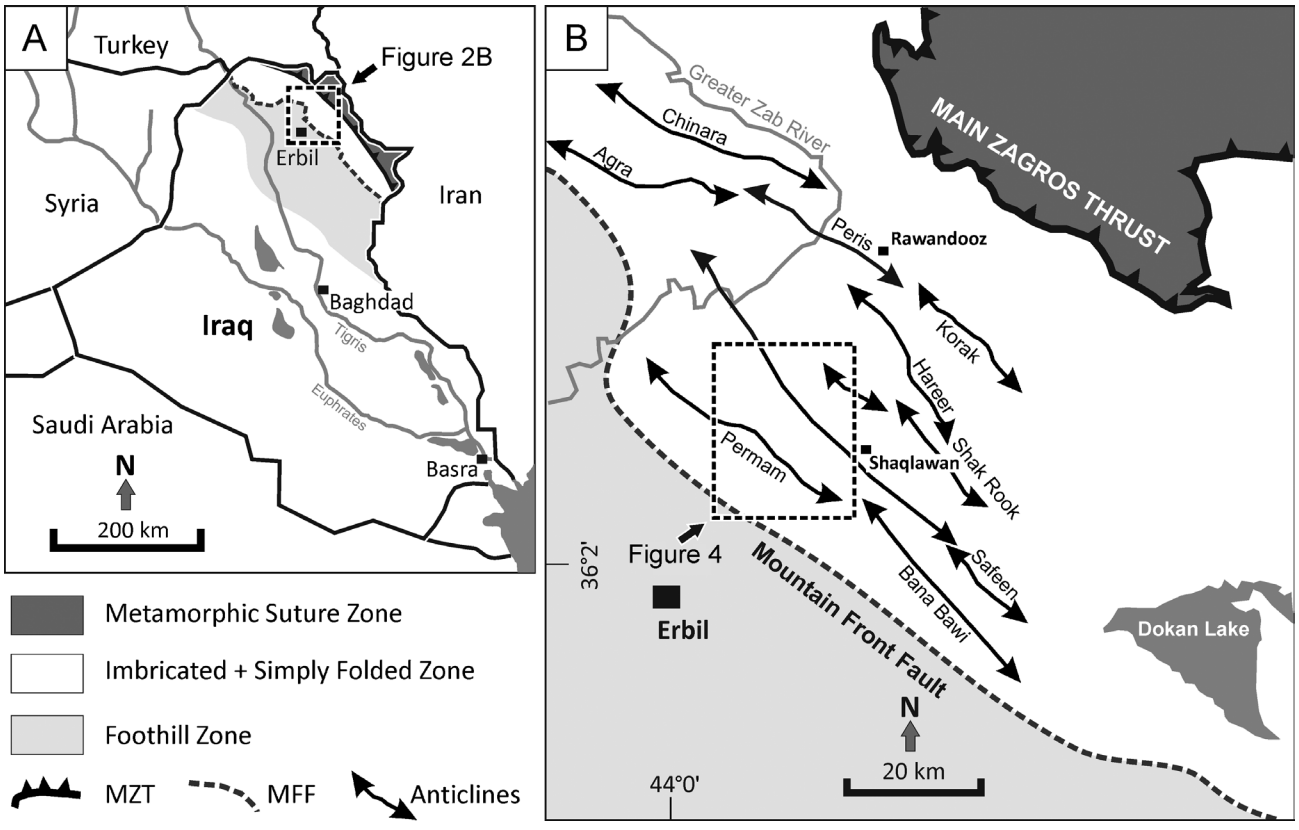

Figure 2. (A) Map of the Republic of Iraq with the major tectonic units of the Zagros Mountains. (B) Map of the tectonic units in the Kurdistan region in northeastern Iraq. Location and names of the major antiforms in the simply folded belt (modified from Reif et al., 2011, used with permission of AAPG). MZT = Main Zagros thrust; MFF = mountain front fault.

The particular focus of this article is the curvature analysis of digital elevation models (DEMs) of the so-called simply folded belt in the northwest Zagros in the Kurdistan region of Iraq. By systematically varying two key parameters of the curvature calculation, the geomorphological signals of various wavelengths can be enhanced.

GEOLOGIC SETTING

The Zagros Mountains, which extend more than 1800 km (>1120 mi) from northern Iraq to the Strait of Hormuz in Iran, are the result of the ongoing collision between the Eurasian and Arabian plates, whose convergence began in the Late Cretaceous (Dewey et al., 1973; Dercourt et al., 1986). The active north-south convergence between these two plates is about 2 cm/yr and is partitioned within the Zagros Mountains in a southwest-directed folding and thrusting, and northwest-southeast– and north-south–trending dextral strike-slip faults (Sella et al., 2002; Vernant et al., 2004). From the suture zone toward the southwest, the Zagros belt consists of four individual tectonic units (Falcon, 1961) (Figure 2): (1) the Sanandaj-Sirjan metamorphic zone, (2) the thrust-dominated imbricated zone, (3) the simply folded belt, and (4) the foothill zone with buried folds. The main Zagros thrust represents the suture zone and borders the imbricated zone toward the northeast. The mountain front fault is the southwestern boundary of the simply folded belt, which has a width of about 25 to 50 km (~15.6–31 mi) in northeastern Iraq (Jassim and Goff, 2006).

This study focuses on the simply folded belt, northeast of the city of Erbil, which is characterized by thin-skinned deformation of a 9- to 10-km (5.6- to 6.2-mi)-thick sedimentary cover above a Precambrian basement. Interestingly, major faults

Figure 3. The Hareer anticline is mainly composed of massive to thick-bedded Cretaceous limestone with local dolomitization. The topographic ridge corresponds directly to the antiformal geologic structure, whereas the synformal part is covered by Quaternary sediments (frontal part of the picture). In the northwestern part of the structure, the topography is controlled by the bedding surface of the folded sediments, but in the central and southeastern parts, the antiformal shape is strongly dissected by the fluviatile drainage system.

are widely absent in this region, and shortening is accommodated by open, upright, and regularly spaced folds, which strike northwest-southeast. The shape of the folds is mainly subcylindrical with wavelengths between 6 and 10 km (3.7–6.2 mi). Most of the antiforms have a flat top resulting in box-shaped folds with two axial planes dipping northeast and southwest. Field measurements of the folded sedimentary beddings suggest that the folds are clearly asymmetric, with steeper southwest-dipping forelimbs and shallower northeast-dipping back limbs (Reif et al., 2011).

In the investigated area, the folded stratigraphy is composed of Cretaceous to Neogene sediments (Sissakian et al., 1997; Bretis et al., 2011). The youngest folded formation is of Pliocene age, which corroborates observations from the Iranian part of the Zagros that the deformation in the simply folded belt started between 8 (Homke et al., 2004) and 5 Ma (Allen et al., 2004). The folded stratigraphy consists of alternating layers of more competent rocks (limestones, dolomite, sandstones) and less competent rocks (marls, shales). The differences in composition of these lithologies result in a considerable variation in weathering resistivity. Therefore, the fold structures significantly control the landscape evolution, and analysis of the topographic data allows drawing conclusions on the underlying geologic structures. The most obvious geomorphological observation in the field is that the anticlines of the simply folded belt directly correspond to topographic ridges, whereas the synclines are covered by Quaternary sediments (Figure 3). In the following, the shapes of the anticlines are investigated from DEM data with a particular focus on the Permam anticline about 30 km (~19 mi) north-northeast of Erbil (Figure 4).

DESCRIPTION OF FOLDED SURFACES USING DIFFERENTIAL GEOMETRY

To compute length, angles, and areas on an arbitrary curved surface, it is necessary to describe its shape in space. A reasonable description of how much a curved surface deviates from a planar surface is given by the powerful mathematical notion of curvature. Intuitively, the calculation of the normal curvature, k, at a given point on the surface can be reduced to the calculation of the curvature of all curves on the surface passing through this point. Such curves are systematically studied by the intersection of the curved surface with planes normal to it. Such a study reveals that the curvature at a given point on a surface is not constant, but is a function of the direction in which it is calculated. Most importantly, however, two distinct so-called principal curvature directions with maximal and minimal curvature values (k_{max} and k_{min}) exist. These two directions are orthogonal to each other and, together with the two corresponding principal curvature values, fully determine the

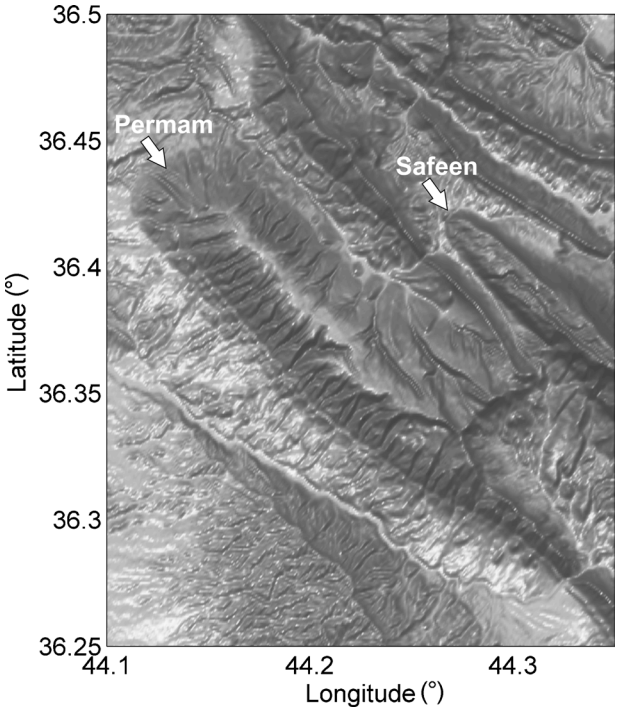

Figure 4. The Shuttle Radar Topography Mission digital elevation model of the Permam and Safeen anticlines.

shape of the surface at this point. For example, a cylinder with radius, r, has a maximal curvature of $1/r$ along the circular sections and a minimal curvature of 0 along the generators.

Fundamental Forms and Shape Operator

In modern differential geometry, the local shape of a surface is characterized by the first and second fundamental forms, I and II, respectively. The first fundamental form, I, is the inner product on the tangent space of the surface and, hence, quantifies intrinsic properties of the surface. The second fundamental form, II, however, describes the change in the normal direction and, hence, is a tool to examine the extrinsic geometry of the surface. The ratio between the first and second fundamental form defines the shape operator, L:

$$L = \mathrm{I}^{-1} \times \mathrm{II} \qquad (1)$$

which describes the infinitesimal change of the normal vector along the surface. Provided that a local description of a surface is available, the coefficients of these three symmetric 2 × 2 tensor fields may be computed at each point of the surface. The precise mathematical background for the computations in this article is sketched in the Appendix and elaborated in Pollard and Fletcher (2005).

Principal Curvatures

The shape operator, L, is the key quantity for curvature computations because it determines the normal curvature, k_w, at a given point, p, on the surface in direction, w:

$$k_w = \mathrm{II}(w, w) = \langle w, L_p(w) \rangle \qquad (2)$$

The principal curvature directions at point p are the eigenvectors of L_p. They form an orthonormal basis on the tangent space, that is, the maximal and minimal curvature directions are normal to each other everywhere on the surface. The eigenvalues of L_p correspond to the minimal and maximal curvature values at point p, k_{min}, and k_{max}, respectively. Principal curvatures are useful to quantify the amount of folding and to identify fold axes and generalized hinge lines (Mynatt et al., 2007; Lisle et al., 2010). The computation of the principal curvature directions and values on a digital surface model using the shape operator, L, is straightforward to implement numerically.

Gaussian Curvature and Mean Curvature

To distinguish different geologic shapes, it is not sufficient to just compute the absolute curvature values. Qualitative descriptions and classifications of geologic surfaces make use of sign changes of the principal curvature values. The Gaussian curvature

$$k_G = k_{min} \times k_{max} = \det(L) \qquad (3)$$

is an entirely intrinsic quantity of a curved surface. For example, on perfectly cylindrical folds, one of the two principal curvatures is always zero and, hence, $k_G = 0$. Therefore, the Gaussian curvature

is a tool to detect noncylindrical shapes, including strained zones and faults. The mean curvature

$$k_M = \frac{k_{min} + k_{max}}{2} = \frac{tr(L)}{2} \quad (4)$$

singles out the dominant curvature value. Only planes and perfect saddles have zero mean curvature. In general situations, the mean curvature highlights the orientation of the surface. Therefore, k_M is a useful quantity to distinguish synformal from antiformal structures.

Geologic Curvature

The geologic curvature classification (Lisle and Toimil, 2007; Mynatt et al., 2007) combines the information from both the Gaussian curvature and the mean curvature and, thus, successfully divides geologic surfaces into areas of structural similarity (Figure 1). Cylindrical fold shapes (synforms, antiforms, and planes) are determined by a vanishing Gaussian curvature. A positive Gaussian curvature implies that all curvature values have the same sign, which is the case for dome and basin structures. Because the Gaussian curvature, however, is an intrinsic quantity, it is not adequate to distinguish between differently aligned shapes in space. The difference between predominantly convex and predominantly concave situations can only be determined by the mean curvature. In geologic terms, the mean curvature separates antiformal shapes from synformal shapes.

Implementation to MATLAB

The curvature analysis of the Permam anticline is based on the differential geometric methods and the geologic curvature classification from Mynatt et al. (2007). The DEMs are obtained from 3 arcsecond Shuttle Radar Topography Mission (SRTM) data sets, where moderately sized null data holes were patched by the program SRTMFill (3D Nature, 2003). These processed DEMs were converted to MATLAB data files using an adopted version of the program GetSRTMData (Hölz, 2004). The numerical curvature computations of the Permam anticline were performed using a modified version of the MATLAB scripts used by Mynatt et al. (2007). As such, the analyses in this article also make use of a spectral filtering method for the DEMs and a variable curvature threshold. A large part of the discussion following the numerical curvature computations for the Permam anticline is devoted to both scale and threshold sensitivity.

Low-Pass Filters Applied to Topographic Data

Before curvatures are calculated, a low-pass filter is applied to the topographic data set, as suggested by Bergbauer and Pollard (2003). This allows suppressing short-wavelength features in the topographic data, such as measurement inaccuracies or very narrow river incisions. Also, by applying a low-pass filter, structures with a long wavelength can be analyzed without the interference of short-wavelength structures. The separation of short-wavelength surface undulations from the main structural content is achieved by cutting off wavelengths shorter than the so-called cutoff wavelength, s, by means of Fourier transform (Bergbauer et al., 2003). By further increasing the cutoff wavelength, it is also possible to suppress topographic features that are caused by small-scale geomorphological processes. This allows enhancing the large-scale tectonic structures (e.g., anticlines) and separating topographic features that are primarily caused by geomorphological processes from those primarily caused by tectonic processes.

Curvature Threshold

In many practical situations, the computed curvature of a surface does not allow for a useful geologic fold classification or interpretation. This is caused by rough natural surfaces, measurement errors, and resolution restrictions of the DEM. To simplify the classification and highlight the dominant structures of naturally folded surfaces, an approximation by cylindrical shapes (i.e., planes, synforms, antiforms; Figure 1) is commonly sufficient. Shapes with only a small deviation from a cylindrical shape are approximated by the corresponding cylindrical shape using the curvature threshold, k_t (Mynatt et al.,

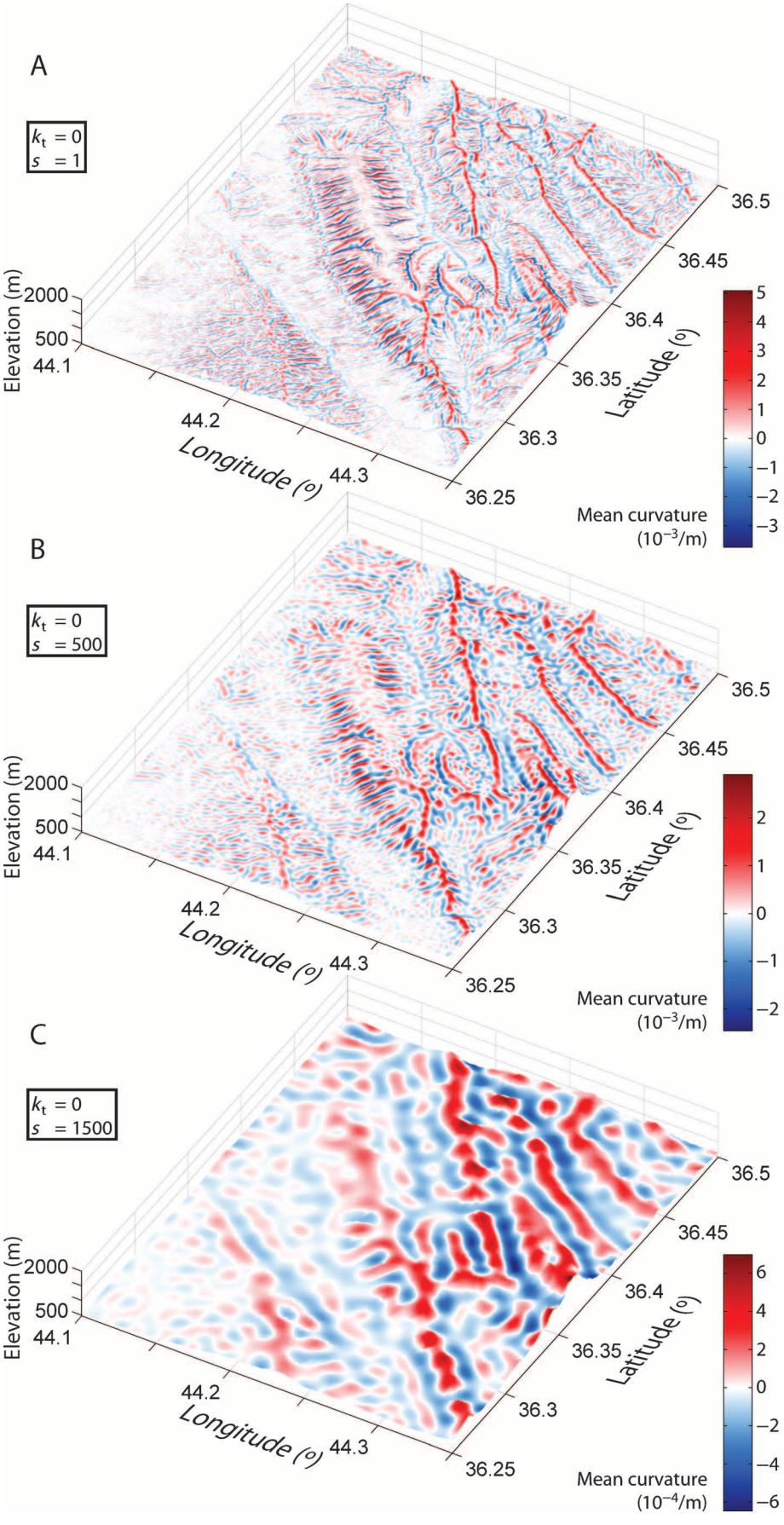

Figure 5. Mean curvature, k_M, of the Permam anticline calculated from the Shuttle Radar Topography Mission (SRTM) topographic data draped onto the 2× exaggerated topography. For the curvature calculation, different low-pass filters (cutoff wavelength, s) are applied. In A, no low-pass filter is applied (s < resolution of SRTM data). In B and C, wavelengths smaller than 500 m (1640 ft) and 1500 m (4921 ft), respectively, are deleted from the SRTM data set. Note the different color scale for the different panels. The curvature threshold, k_t, is set to zero.

2007). Thereby, principal curvatures with an absolute value below k_t are set to zero:

$$\text{if } |k| < k_t \text{ then } k = 0 \quad (5)$$

Saddle points with a shape close to a perfect saddle are approximated by a perfect saddle using the alternative condition $|k_{max} + k_{min}| < k_t$ in the above statement. Subsequently, a non-zero curvature threshold also affects the mean, Gaussian, and geologic curvatures, leading to bigger areas of cylindrical geologic shapes. Thus, by increasing the value of k_t, structures are simplified with respect to the geologic curvature classification.

CURVATURE ANALYSIS OF THE PERMAM ANTICLINE

To analyze the Permam anticline, the freely available SRTM data with 3 arc-second resolution (~90 m [~295 ft]) was used. The Permam anticline is particularly well suited for a curvature analysis based on topographic data because the level of erosion is generally within the relatively competent limestone of the Pilaspi Formation (Reif et al., 2011). Therefore, the Permam anticline resists erosion more effectively than other regional anticlines, and the topography generally follows the structure of the anticline (Bretis et al., 2011; Reif et al., 2011).

Scale Sensitivity

By applying a low-pass filter with different cutoff wavelengths to the SRTM data set, structures on different scales can be made visible. Figure 5 shows the mean curvature, k_M, for applied cutoff wavelengths of s = 1 m (3.3 ft) (no low-pass filter), s = 500 m (1640 ft), and s = 1500 m (4921 ft). A negative mean curvature highlights a concave topography (synclines and basins), and a positive mean curvature highlights a convex topography (anticlines and domes). With no low-pass filter applied (Figure 5A), the Permam anticline is dominated by erosion structures (narrow river incisions) perpendicular to the fold axis, but the large-scale anticlinal structure is not very visible. This pattern suggests that the Permam anticline is relatively flat in its hinge area, almost forming a topographic plateau, and eroded at its limbs by incisions arranged perpendicular to the fold axes. At the nose of the antiform, the radial drainage pattern is clearly visible, but the incisions are not as strongly developed as on the fold limbs, leading to smaller curvature values. In some places, more competent layers lying on top of less competent layers (e.g., carbonates on top of marls) show stronger resistivity to erosion and, hence, form hogbacks (i.e., homoclinal ridges that form because of lithologic contrasts and different weathering rates). The outlines of these hogbacks (e.g., at the limbs of the Safeen anticline) have sharp edges and, therefore, are nicely visualized by large positive k_M values. Using a cutoff wavelength for the low-pass filter of s = 1500 m (4921 ft) (Figure 5C) strongly reduces the influence of local erosion structures at the limbs of the Permam anticline, and the large-scale anticlinal structure is emphasized by positive k_M values. The core of the Safeen anticline is also very visible in the same way, but the hogbacks on the flanks of the Safeen anticline are still present. Throughout the entire investigation area, the northwest-southeast–trending fold traces are hardly interrupted by erosion structures perpendicular to this trend. The intermediate cutoff wavelength of s = 500 m (1640 ft) reveals a mixture between the two extreme cases described above. This intermediate-value low-pass filter is used for the following investigation.

Sensitivity on Threshold Value (Curvature Threshold)

Using the geologic fold classification based on the full value range for the Gaussian and mean curvatures (Mynatt et al., 2007; Figure 1) results in Figure 6C. Although the Gaussian (Figure 6A) and mean curvatures (Figure 6B) themselves reveal several details, the geologic fold classification appears rather tessellated and is virtually unusable. Therefore, the threshold value k_t was applied to the principal curvatures k_{min} and k_{max} before calculating the Gaussian, mean, and geologic curvatures. Figure 6 shows the effect of an increasing

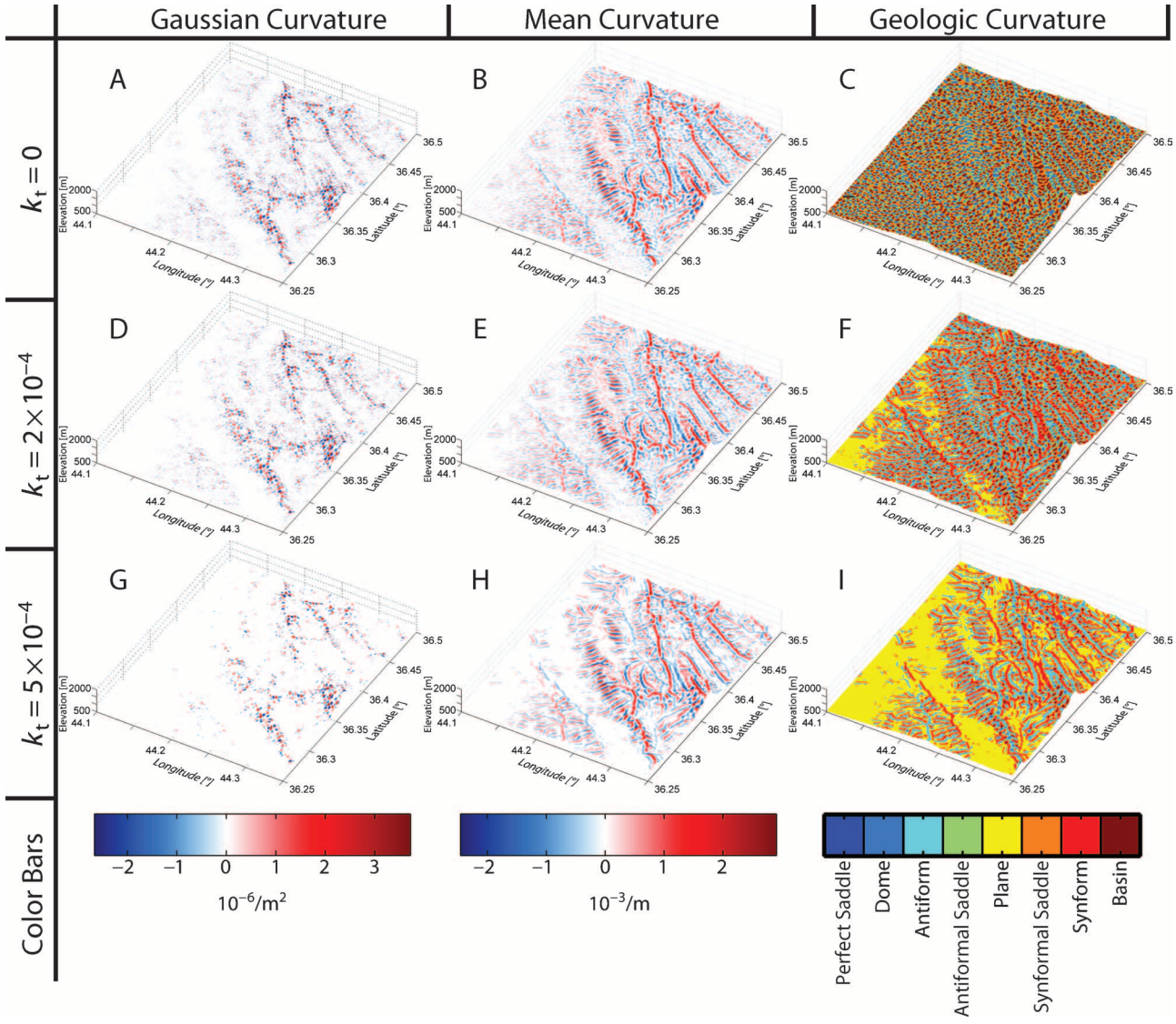

Figure 6. Gaussian, mean, and geologic curvature of the Permam Anticline calculated from the Shuttle Radar Topography Mission (SRTM) topographic data draped onto the 2× exaggerated topography. For the curvature calculation, different threshold values, k_t (1/m), are applied. (A–I) A low-pass filter with a cutoff wavelength of s = 500 m (1640 ft) is applied to the SRTM data set.

threshold value on the Gaussian, mean, and geologic curvatures. For the Gaussian and mean curvatures, an increasing threshold value corresponds to a whitening of the curvature maps. In other words, information appears to be lost with an increasing threshold value. However, the geologic curvature map (Figure 6C, F, and I) shows the opposite effect: the tessellated map becomes clearer with an increasing threshold value. At low threshold values (Figure 6C), all geologic fold classifications occur with a short space between each other, which leads to the tessellated and less informative appearance. With an increasing threshold value, two effects occur: (1) larger and more systematically connected areas are classified as the same, and (2) the cylindrical classifications (antiform, synform, plane) appear more commonly than the three-dimensional (3-D) classifications (dome, basins, all types of saddles). These two effects lead to a more coherent geologic curvature map, which is easier to interpret than the tessellated original map with a small threshold value. Note that all panels in Figure 6 are calculated with the same cutoff wavelength of the low-pass filter. Therefore, the readability of the

geologic curvature maps is independent of the resolution or scale of the topographic data, but is solely caused by the increase in the threshold value, k_t.

DISCUSSION

Classical geologic descriptions of folded surfaces rely on the assumption that folds are cylindrical. Geologic surfaces, however, do not follow a perfect antiform-synform pattern, and a lot of the geometric information is lost if simplistic descriptions are used. By using remote sensing data, such as SRTM, large areas can be studied by 3-D curvature analysis. The presented curvature analysis of surface data of the Permam and Safeen anticlines demonstrates that the calculated mean, Gaussian, and geologic curvatures can be used for both geomorphological and tectonic interpretations. Crucial for separating topographic features of different wavelengths is a proper adjustment of the parameters that influence the spectral content of the topographic data (i.e., low-pass filter applied to the DEM) and the readability (i.e., the threshold applied to the principal curvatures) of the analysis.

Separation of Geomorphological and Structural Features

In the presented example, small-scale geomorphological processes, such as river incisions, dominate the mean curvature distribution up to wavelengths of about 500 m (~1640 ft) (Figure 5A, B). On this scale, high positive and negative curvature values are associated with intense erosion and high future erosion potential (e.g., Simpson, 2009). Areas with a high positive mean curvature are more exposed to weathering and, hence, more prone to erosion, whereas sedimentation primarily occurs in areas with a negative mean curvature. On a larger scale, the synclines already appear flat (low negative curvature) as they are covered by Quaternary sediments. In the same study area, small-scale surface drainage patterns have been used successfully by Bretis et al. (2011) to study fold growth and evolution. Curvature analysis can support and simplify such field-based studies. Indeed, the observations of the drainage pattern and of the hogbacks based on the mean curvature distribution made in this study are in accordance with the field-based observations in the same area (Bretis et al., 2011).

The large-scale tectonic structures are best studied by cutting off wavelengths shorter than 1500 m (4921 ft) (Figure 5C). On this scale, some areas of positive mean curvature correspond to anticlinal hinges (e.g., the Permam anticline). However, a tectonic interpretation solely based on curvature analysis can be misleading because erosional surface features are also present on the large scale (i.e., >1500 m [>4921 ft]). For example, the Safeen anticline emerges as three subparallel ridges of high positive curvature values. The two external ridges correspond to hogbacks, and only the central ridge corresponds to the anticlinal hinge. Hence, the geologic curvature classification (Figure 1) of the surface topography does not necessarily correspond to the actual tectonic structures. Geologic background knowledge and fieldwork are necessary to correctly interpret the curvature analysis.

On the large scale, the surface topography generally follows the tectonic anticlinal structures in the study area, whereas on the small scale, the topography is dominated by a strong erosional overprint. However, the wavelength spectra of these two different types of structures (i.e., tectonic vs. geomorphological) clearly overlap. Therefore, a complete separation cannot be achieved, but an emphasis of either of the two is feasible by suppressing certain wavelengths. The wavelength threshold appropriate for analyzing either tectonic or geomorphological structure depends on the regional geology and erosional conditions, and no general rule can be given here. We, therefore, recommend that one carefully studies curvature distributions with various parameter settings and relates them to observations in the field.

Geologic Curvature

The geologic curvature becomes more useful with increasing threshold values because larger and more systematically connected areas are classified as the same geologic shapes. Therefore, the quality of a geologic curvature map mainly depends on two

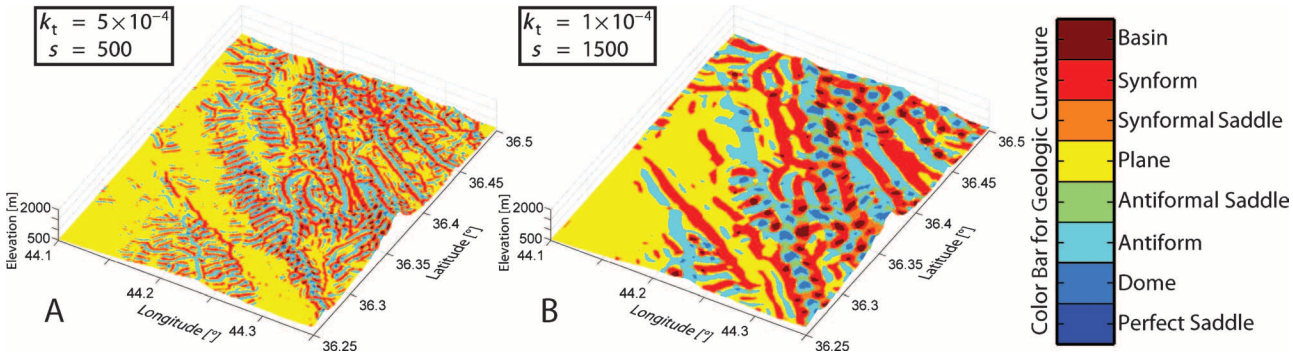

Figure 7. Geologic curvature of the Permam anticline calculated from the Shuttle Radar Topography Mission topographic data draped onto the 2× exaggerated topography. For the curvature calculation, different low-pass filters (cutoff wavelength, *s*, here in m) and different threshold values, k_t (here in 1/m), are applied.

parameters: (1) the cutoff wavelength, *s*, of the low-pass filter and (2) the threshold value, k_t. To demonstrate the effect of the combination of these two parameters, the geologic curvature is calculated using two different optimal parameter couples. In Figure 7A, the cutoff wavelength, *s*, is chosen to enhance small-scale geomorphological features and the threshold value, k_t, is selected to highlight geomorphological features with strong curvatures. Resulting from this combination, erosional features, such as deeply incised river valleys or sharp ridges, are strongly enhanced. In Figure 7B, the parameters were selected to highlight topographic features related to the larger scale tectonic fold structures, which have a wavelength of about 6 to 10 km (~3.7–6.2 mi) and an amplitude of 0.5 to 1 km (0.3–0.6 mi). Erosional features with a much shorter wavelength, especially the narrowly spaced drainage pattern perpendicular to the fold axes, are successfully filtered out by this combination of parameters. The geologic curvature map predominantly displays antiforms, synforms, and planes. Both the Permam and the Safeen anticlines are correctly outlined by the geologic curvature maps. The hinge areas are relatively broad because of the boxlike shape of the anticlines. The limbs of the Permam anticline are mapped as planes, reflecting the shape of the relatively straight limbs. The Safeen anticline is flanked by two straight subparallel structures that are mapped as antiforms. However, these structures are not antiforms, but hogbacks flanking the antiform. This confirms that a tectonic interpretation solely based on curvature analysis can be misleading, as discussed above. The synclines to the northwest and southeast of the Permam anticline are mapped as planes, which is a result of the Quaternary deposit in the synformal areas.

Although the tectonic and the geomorphological signatures cannot be separated completely, as in the case of mean curvature analysis, these examples of two different optimal parameter configurations may be used for different applications. Figure 7A may be used to analyze the river network and to draw conclusions on, for example, the magnitude of the river incision or the development of the drainage network during fold growth. Figure 7B may also be used to analyze the large-scale folding style or to correlate these surface data with reflection seismic data of the underlying structures.

Applications to Subsurface Data

Curvature analysis of the surface topography is a simple and quick ad hoc tool to visualize and quantify geologic structures and draw first conclusions regarding geologic processes. Although DEM analysis cannot replace fieldwork and should not be considered independently, curvature analysis can serve as a guide for further investigations and, hence, render it useful for the hydrocarbon industry. Note that curvature analysis is certainly not restricted to topographic data. For example, it can equally well be applied to seismically mapped surfaces in 3-D seismic data sets (Roberts, 2001; Mynatt et al., 2007). Obviously, erosional effects do not play a

role when analyzing seismically mapped surfaces with short wavelengths, which allows a true structural geologic interpretation on different scales using differential geometry. If it is assumed that layers of rock deform like elastic plates so that layer-parallel stresses are directly related to the curvature of the folded surface, curvature analysis might be used to predict the location and characteristics of fracture networks in folded rock layers (e.g., Stearns and Friedman, 1972, Fischer et al., 1992; Storti and Salvini, 2001). Moreover, a detailed 3-D curvature analysis of seismically mapped surfaces could be used for locating potential traps, studying their geometry (spill points, etc.) and estimating the maximal possible reservoir volume of a trap (Mynatt et al., 2007). Such direct applications to seismic data reveal the great potential of curvature analysis in view of hydrocarbon exploration. To gain insight in the vertical continuation of geologic structures, it is suggested that studies of seismic reflectors are combined with curvature analysis of topographic data above the seismic 3-D cube.

CONCLUSIONS

Curvature analysis of DEMs from the Zagros fold and thrust belt in northern Iraq demonstrates the importance of adjusting two key parameters that control the visualization of topographic features of various wavelengths. First, a low-pass filter applied to the topographic data allows the suppression of features below a critical wavelength. Second, a threshold value controls how the geologic curvature classes are mapped in the investigated area, that is, strongly alternating versus larger connected areas of the same geologic curvature classes. Both parameters can be adjusted to either display small-scale geomorphological features with high curvature values (like incised river gorges or edges of hogbacks) or large-scale bending of surfaces (e.g., the shape of an antiform). Because the filter and threshold value influence each other, it is crucial, but not straightforward, to adjust them properly for the highest information content of the results. Structural interpretation solely based on curvature analysis can be misleading without geologic background knowledge and fieldwork.

The Gaussian curvature alone carries the least information. The mean curvature is a useful tool to investigate the orientation pattern of geomorphological features. Combined, the geologic curvature is an ideal mapping tool to intuitively display the shape characteristics of geologic structures.

APPENDIX: MATHEMATICAL BACKGROUND FOR CURVATURE COMPUTATIONS

Let $\{\mathbf{e}_x = (1,0,0), \mathbf{e}_y = (0,1,0), \mathbf{e}_z = (0,0,1)\}$ denote the standard basis in the 3-D Euclidean space $\mathbb{R}^3$. Suppose U is an open subset of the Euclidean plane $\mathbb{R}^2$. Let u: $U \rightarrow \mathbb{R}^3$ be a local parameterization of a (hyper)surface, M, given by

$$\mathbf{u}(s,t) = s\mathbf{e}_x + t\mathbf{e}_y + z(s,t)\mathbf{e}_z$$

Thus, for any fixed point (s, t) of the plane, $z(s, t)$ describes the elevation of the surface and $\mathbf{u}(s, t)$ = (s,t,z(s,t)) the corresponding point in space. For any given point, p, on the surface, M, the tangent space to the surface shall be denoted by $T_\mathrm{p}\mathrm{M}$. Two linearly independent tangent vectors at each point of the surface are naturally provided by the derivatives of the parameterization, $\mathbf{u}$ (the indices s and t indicate the corresponding partial derivatives of $\mathbf{u}$ and z):

$$\mathbf{u}_s = \frac{\partial \mathbf{u}}{\partial s} = (1,0,z_s) \text{ and } \mathbf{u}_t = \frac{\partial \mathbf{u}}{\partial t} = (0,1,z_t)$$

They automatically form a basis for the tangent spaces, $T_\mathrm{p}\mathrm{M}$, at all points, p, of the surface and are, therefore, useful quantities for further tensor calculations.

The first fundamental form, I, is a tensor field defined by the inner product of the tangent space (which is canonically induced from the standard inner product of the 3-D Euclidean space):

$$\mathrm{I}_\mathrm{p}(v,w) = \langle v,w\rangle \text{ for } v,w \in T_\mathrm{p}\mathrm{M}$$

This is an inherently intrinsic quantity of the surface, M. The extrinsic information is essentially contained in the Gauss map, n, a vector field that assigns to each point, p, on the surface the positively oriented unit normal vector, n_p. The shape operator, L, is the tangent map, Tn of n and, hence, quantifies the infinitesimal directional change of these normal vectors, n, along the surface. It is crucial for curvature computations because the normal curvature, k_w, at a point, p, in direction $w \in T_\mathrm{p}\mathrm{M}$ is given by

$$k_\mathrm{w}(\mathrm{p}) = \langle w, \mathrm{T}_\mathrm{p}\mathrm{n}(w)\rangle = \langle w, \mathrm{L}_\mathrm{p}(w)\rangle$$

The second fundamental form, II, is precisely this infinitesimal change of the normal vectors, n, to the surface in the tangential directions, that is

$$\mathrm{II}_p(v,w) = \langle v, T_p n(w) \rangle \text{ for } v, w \in T_p \mathrm{M}$$

Using the local parameterization, $\mathbf{u}$, introduced above, the first and second fundamental forms can be expressed with respect to the tangent basis vectors $\mathbf{u}_s$ and $\mathbf{u}_t$ and second derivatives $\mathbf{u}_{ss}, \mathbf{u}_{st} = \mathbf{u}_{ts}, \mathbf{u}_{tt}$ and normal vector $n = \frac{\mathbf{u}_s \times \mathbf{u}_t}{|\mathbf{u}_s \times \mathbf{u}_t|}$, respectively:

$$\mathrm{I} = \begin{pmatrix} E & F \\ F & G \end{pmatrix} \text{ and } \mathrm{II} = \begin{pmatrix} e & f \\ f & g \end{pmatrix}$$

with coefficients

$$E = \langle \mathbf{u}_s, \mathbf{u}_s \rangle = 1 + z_s^2$$

$$e = -\langle \mathbf{u}_{ss}, n \rangle = -\frac{\det(\mathbf{u}_s, \mathbf{u}_t, \mathbf{u}_{ss})}{\sqrt{EG - F^2}} = -\frac{z_{ss}}{\sqrt{1 + z_s^2 + z_t^2}}$$

$$F = \langle \mathbf{u}_s, \mathbf{u}_t \rangle = \langle \mathbf{u}_t, \mathbf{u}_s \rangle = z_s + z_t$$

$$f = -\langle \mathbf{u}_{st}, n \rangle = -\frac{\det(\mathbf{u}_s, \mathbf{u}_t, \mathbf{u}_{st})}{\sqrt{EG - F^2}} = -\frac{z_{st}}{\sqrt{1 + z_s^2 + z_t^2}}$$

$$G = \langle \mathbf{u}_s, \mathbf{u}_t \rangle = 1 + z_2^t$$

$$g = -\langle \mathbf{u}_{tt}, n \rangle = -\frac{\det(\mathbf{u}_s, \mathbf{u}_t, \mathbf{u}_{tt})}{\sqrt{EG - F^2}} = -\frac{z_{tt}}{\sqrt{1 + z_s^2 + z_t^2}}$$

and normal vector $n = \frac{\mathbf{u}_s \times \mathbf{u}_t}{|\mathbf{u}_s \times \mathbf{u}_t|} = \frac{\mathbf{u}_s \times \mathbf{u}_t}{\sqrt{EG - F^2}}$. It can be shown that the shape operator is the ratio between I and II, that is,

$$L = \mathrm{I}^{-1} \times \mathrm{II} = \frac{1}{EG - F^2} \begin{pmatrix} eG - fF & fG - gF \\ fE - eF & gE - fF \end{pmatrix}$$

The eigenvalues and eigenvectors of L are the extreme normal curvature values, $k_{\min}$ and $k_{\max}$, and the corresponding principal curvature directions. Alternatively, these quantities can be computed from the Gaussian curvature, k_G, and mean curvature, k_M:

$$k_G = \det \mathrm{L} = \frac{eg - f^2}{EG - F^2}$$

$$k_M = \frac{\mathrm{tr\,L}}{2} = \frac{Ge - 2fF + Eg}{2(EG - F^2)}$$

$$k_{\max,\min} = k_M \pm \sqrt{k_M^2 - k_G}$$

REFERENCES CITED

3D Nature, 2003, SRTMFill: http://3dnature.com/srtmfill.html (accessed December 5, 2009).

Allen, M., J. Jackson, and R. Walker, 2004, Late Cenozoic reorganization of the Arabia-Eurasia collision and the comparison of short-term and long-term deformation rates: Tectonics, v. 23, p. TC2008, doi:10.1029/2003TC001530.

Bergbauer, S., and D. D. Pollard, 2003, How to calculate normal curvatures of sampled geological surfaces: Journal of Structural Geology, v. 25, p. 277–289, doi:10.1016/S0191-8141(02)00019-6.

Bergbauer, S., T. Mukerji, and P. H. Hennings, 2003, Improving curvature analyses of deformed horizons using scale-dependent filtering techniques: AAPG Bulletin, v. 87, p. 1255–1272, doi:10.1306/0319032001101.

Bretis, B., N. Bartl, and B. Grasemann, 2011, Lateral fold growth and linkage in the Zagros fold and thrust belt (Kurdistan, NE Iraq): Basin Research, first published online April 4, 2011, doi:10.1111/j.1365-2117.2011.00506.x.

Dercourt, J., et al., 1986, Geological evolution of the Tethys belt from the Atlantic to the Pamirs since the Lias: Tectonophysics, v. 1–4, p. 241–315, doi:10.1016/0040-1951(86)90199-X.

Dewey, J. F., W. C. Pitman, W. B. F. Ryan, and J. Bonnin, 1973, Plate tectonics and the evolution of the Alpine system: Geological Society of America Bulletin, v. 84, p. 3137–3180, doi:10.1130/0016-7606(1973)84<3137:PTATEO>2.0.CO;2.

Falcon, N. L., 1961, Major earth-flexuring in the Zagros Mountains of southwest Iran: Quarterly Journal of the Geological Society of London, v. 117, p. 367–376, doi:10.1144/gsjgs.117.1.0367.

Fernandez-Martínez, J. L., and R. J. Lisle, 2009, GenLab: A MATLAB-based program for structural analysis of folds mapped by GPS or seismic methods: Computers and Geosciences, v. 35, p. 317–326, doi:10.1016/j.cageo.2008.08.001.

Fischer, M. P., and M. S. Wilkerson, 2000, Predicting the orientation of joints from fold shape: Results of pseudo-three-dimensional modeling and curvature analysis: Geology, v. 28, p. 15–18, doi:10.1130/0091-7613(2000)28<15:PTOOJF>2.0.CO;2.

Fischer, M. P., N. B. Woodward, and M. M. Mitchell, 1992, The kinematics of break-thrust folds: Journal of Structural Geology, v. 14, p. 451–460, doi:10.1016/0191-8141(92)90105-6.

Hennings, P. H., J. E. Olson, and L. B. Thompson, 2000, Combining outcrop data and three-dimensional structural models to characterize fractured reservoirs: An example from Wyoming: AAPG Bulletin, v. 84, p. 830–849.

Hölz, S., 2004, GetSRTMData: http://www.mathworks.com/matlabcentral/fileexchange/5544-getsrtmdata (accessed December 5, 2009).

Homke, S., J. Vergés, M. Garcés, H. Emami, and R. Karpuz, 2004, Magnetostratigraphy of Miocene–Pliocene Zagros foreland deposits in the front of the Push-e Kush arc (Lurestan Province, Iran): Earth and Planetary Science Letters, v. 225, p. 397–410, doi:10.1016/j.epsl.2004.07.002.

Jassim, S. Z., and J. C. Goff, 2006, Geology of Iraq: Dolin, Prague and Moravian Museum, Berno, 352 p.

Johnson, K. M., and A. M. Johnson, 2000, Localization of layer-parallel faults in San Rafael swell, Utah and other monoclinal folds: Journal of Structural Geology, v. 22, p. 1455–1468, doi:10.1016/S0191-8141(00)00046-8.

Jordan, G., 2003, Morphometric analysis and tectonic interpretation of digital terrain data: A case study: Earth Surface

Processes and Landforms, v. 28, p. 807–822, doi:10.1002/esp.469.
Lacombe, O., J. Lavé, F. Roure, and J. Verges, 2007, Thrust belts and foreland basins: From fold kinematics to hydrocarbon systems: Berlin, Springer-Verlag, Frontiers in Earth Sciences Series, v. XXIV, 492 p.
Lisle, R. J., 1994, Detection of zones of abnormal strains in structures using Gaussian curvature analysis: AAPG Bulletin, v. 78, p. 1811–1819.
Lisle, R. J., 2004, Geological structures and maps: Burlington, Elsevier Butterworth-Heinmann, 106 p.
Lisle, R. J., and J. M. Robinson, 1995, The Mohr circle for curvature and its application to fold description: Journal of Structural Geology, v. 17, p. 739–750, doi:10.1016/0191-8141(94)00089-I.
Lisle, R. J., and N. C. Toimil, 2007, Defining folds on three-dimensional surfaces: Geology, v. 35, p. 519–522, doi:10.1130/G23207A.1.
Lisle, R. J., N. C. Toimil, J. Aller, N. Bobillo-Ares, and F. Bastida, 2010, The hinge lines of non-cylindrical folds: Journal of Structural Geology, v. 32, p. 166–171, doi:10.1016/j.jsg.2009.10.011.
Mynatt, I., S. Bergbauer, and D. D. Pollard, 2007, Using differential geometry to describe 3-D folds: Journal of Structural Geology, v. 29, p. 1256–1266, doi:10.1016/j.jsg.2007.02.006.
Pollard, D. D., and R. C. Fletcher, 2005, Fundamentals of structural geology: Cambridge, Cambridge University Press, 512 p.
Reif, D., B. Grasemann, and R. H. Faber, 2011, Quantitative structural analysis using remote sensing data: Kurdistan, northeast Iraq: AAPG Bulletin, v. 95, p. 941–956, doi:10.1306/11151010112.
Ries, A. C., R. W. H. Butler, and R. H. Graham, 2007, Deformation of the continental crust: The legacy of Mike Coward: Geological Society (London) Special Publication 272, 608 p.
Roberts, A., 2001, Curvature attributes and their application to 3-D interpreted horizons: First Break, v. 19, p. 85–100, doi:10.1046/j.0263-5046.2001.00142.x.
Samson, P., and J.-L. Mallet, 1997, Curvature analysis of triangulated surfaces in structural geology: Mathematical Geology, v. 29, p. 391–412, doi:10.1007/BF02769642.
Sella, G. F., T. H. Dixon, and A. Mao, 2002, REVEL: A model for Recent plate velocities from space geodesy: Journal of Geophysical Research, v. 107, no. B4, doi:10.1029/2000JB000033.
Simpson, G. D. H., 2009, Mechanical modeling of folding versus faulting in brittle-ductile wedges: Journal of Structural Geology, v. 31, p. 369–381, doi:10.1016/j.jsg.2009.01.011.
Sissakian, V. K., E. I. Ibrahim, and I. J. Al-Waily, 1997, Geological map of Arbeel and Mahabad quadrangles: Baghdad, State Establishment of Geological Survey and Mining, Series of Geological Maps of Iraq, scale 1:250,000, 2 sheets.
Stearns, D. W., and M. Friedman, 1972, Reservoirs in fractured rock, *in* R. E. King, ed., Stratigraphic oil and gas fields: Classification, exploration methods, and case histories: AAPG Memoir 16, p. 82–106.
Stephenson, B., A. Koopman, H. Hillgartner, H. McQuillan, S. Bourne, J. Noad, and K. Rawnsley, 2007, Structural and stratigraphic controls on fold-related fracturing in the Zagros Mountains, Iran: Implications for reservoir development, *in* L. Lonergan, R. Jolly, K. Rawnsley, and D. Sanderson, eds., Fractured reservoirs: Geological Society (London) Special Publication 270, p. 1–21.
Storti, F., and F. Salvini, 2001, The evolution of a model trap in the central Apennines, Italy: Fracture patterns, fault reactivation and development of cataclastic rocks in carbonates at the Narni anticline: Journal of Petroleum Geology, v. 24, p. 171–190, doi:10.1111/j.1747-5457.2001.tb00666.x.
Vernant, P., et al., 2004, Present-day crustal deformation and plate kinematics in the Middle East constrained by GPS measurements in Iran and northern Oman: Geophysical Journal International, v. 157, p. 381–398, doi:10.1111/j.1365-246X.2004.02222.x.